INTERNATIONAL JOURNAL OF HYDROGEN ENERGY 41 (2016) 9627–9637

Available online at www.sciencedirect.com

ScienceDirect

journal homepage: www.elsevier.com/locate/he

Anode fabrication for solid oxide fuel cells: Electroless and electrodeposition of nickel and silver into doped ceria scaffolds

Zadariana Jamil [a,b,*], *Enrique Ruiz-Trejo* [a], *Paul Boldrin* [a], *Nigel P. Brandon* [a]

[a] *Department of Earth Science and Engineering, Imperial College London, SW7 2AZ, UK*

[b] *Faculty of Civil Engineering, Universiti Teknologi MARA Pahang, 26400, Bandar Pusat Jengka, Pahang, Malaysia*

ARTICLE INFO

Article history:
Received 19 January 2016
Received in revised form
4 April 2016
Accepted 9 April 2016
Available online 1 May 2016

Keywords:
Solid oxide fuel cell
Electroless
Electrodeposition
Anode fabrication
Ni/GDC

ABSTRACT

A novel fabrication method using electroless and electrodeposited Ni/Ag/GDC for SOFC anodes is presented. First a porous $Ce_{0.9}Gd_{0.1}O_{2-x}$ (GDC) scaffold was deposited on a YSZ electrolyte by screen printing and sintering. The scaffold was then metallized with silver using Tollens' reaction, followed by electrodeposition of nickel from a Watt's bath. The electrodes (Ni/Ag/GDC) were tested in both symmetrical and fuel cell configurations. The microstructures of the Ni/Ag/GDC anodes were analyzed using scanning electron microscopy (SEM) and energy dispersive x-ray spectroscopy (EDX). Nano-particles of Ni formed in the porous GDC scaffold provided triple phase boundaries (TPB). The electronic conductivity of the Ni/Ag/GDC (3.5/24.7/71.8 vol%) electrode was good even at relatively low Ni volume fractions. The electrochemical performance was examined in different concentrations of humidified hydrogen (3% H_2O) and over a range of temperatures (600–750 °C). The total area specific resistance (ASR) of the anode at 750 °C in humidified 97 vol% H_2 was 1.12 Ω cm^2, with low-frequency polarization (R_l) as the largest contributor. The electrodes were successfully integrated into a fuel cell and operated in both H_2 and syngas.

Introduction

Solid oxide fuel cells (SOFCs) could play a significant role in sustainable energy futures because of their ability to convert a diverse range of fuels to electricity at high efficiency. A typical SOFC consists of dense yttria-stabilized zirconia (YSZ) as the oxygen anion conducting electrolyte and Ni-cermets as the anode. A variety of materials are used as the cathode, including doped manganites, cobaltites and ferrites. Ni is usually chosen as the metallic component of the anode because of its high electronic conductivity and stability, excellent reforming characteristics, and good electrocatalytic activity for electrochemical oxidation [1]. However, Ni can catalyze the deposition of carbon on its surface when hydrocarbon fuels are used, leading to cell deactivation under some conditions [2,3].

The performance of SOFC anodes is linked to the length of the triple phase boundary (TPB), where the electrochemical reactions occur. This region is dependent upon the optimization of anode porosity, microstructure and composition [4].

* *Corresponding author*. Department of Earth Science and Engineering, Imperial College London, SW7 2AZ, UK.
E-mail address: z.jamil13@imperial.ac.uk (Z. Jamil).

http://dx.doi.org/10.1016/j.ijhydene.2016.04.061

The reaction sites can also be extended by using Ni/$Ce_{0.9}Gd_{0.1}O_{2-x}$ (Ni/GDC) as compared to the widely used Ni/YSZ anode materials. GDC exhibits mixed ionic and electronic conductivity in the reducing conditions found in an SOFC anode, providing a GDC/gas interface or so-called double-phase boundary (2 PB) that shows electrocatalytic activity [5–7]. Moreover, GDC has the ability to enhance the electrocatalysis of hydrocarbon oxidation, and enables improved sulfur tolerance, via the Ce^{4+}/Ce^{3+} redox transition. It also exhibits higher ionic conductivity than YSZ in the temperature range from 300 to 700 °C [8–13].

Ni/GDC anodes are commonly prepared by mechanically mixing powders of NiO and GDC, followed by sintering at ~1300 °C and reducing in a hydrogen rich atmosphere [14,15] However, this method requires a large volume of Ni (>30 vol %) to achieve adequate electronic conductivity in the electrodes. The impregnation or infiltration method enables the formation of nano-sized oxide or metal particles uniformly in a porous scaffold matrix [16–18]. It allows the fabrication of anode and cathode composites with a wide range of compositions, particularly with metals that cannot be processed at high temperature (e.g. Cu) [19]. However, the impregnation method is time consuming as it requires multiple steps to achieve sufficient conductivity and hence may not be suitable for mass production. Based on previous studies, ten successive metal impregnation steps were required to achieve sufficient electronic conductivity throughout the electrode, demanding more than 10 h for cell fabrication [20–22]. A faster impregnation-irradiation technique (60 s/cycle) to accelerate conventional impregnation methods has shown well distributed Ni in the scaffold, however, repeated cycles can damage the thin scaffolds [23]. Therefore in this paper, we metallize the scaffold by electroless and electrodeposition as an alternative to impregnation as a fabrication method of scaffold electrodes.

Metallizing the scaffold by electroless and electrodeposition methods could be a scalable process due to its ability to add a large amount of metal (including the low melting point metals) to the porous ceramic scaffold in a fast process. An electroless deposition involves chemically reducing metallic ions or complexes onto a substrate in a controlled fashion [24]. Electrodeposition is a versatile technique since a metallic coating is obtained on the surface of another metal or conductive surface by the electroreduction of metal ions from aqueous solutions [25]. This approach allows control of the morphology of metal deposits and may be particularly useful for the production of multilayer microstructures.

Electroless Ni deposition onto YSZ particles for Ni/YSZ cermet anode fabrication has been carried out in several studies [26–28]. Among these studies, the lowest Ni content that has been reported to result in sufficient electrical conductivities for SOFC anode application is 20% vol Ni (~160 S cm^{-1} at 750 °C) [26]. However, their development as SOFC anodes is still at an early stage.

Electrodeposition techniques for SOFC anode fabrication are usually applied to provide bimetallic electrodes especially to avoid carbon formation. It has been shown that this technique is a promising way to add Cu into porous Ni-based anodes at low temperature (<100 °C) to suppress carbon deposition when direct hydrocarbon fuels are used in the SOFC [19,29]. Electrodeposition requires a conducting surface. This can be prepared by several techniques, for example exposing *n*-butane onto scaffolds at elevated temperature (850 °C) to form an electrically conducting carbon layer [30], or pre-incorporating ceramic-metallic composites (Ni/YSZ cermets) [29]. In this study, we focused on the fabrication of Ni/GDC anodes using a combination of electroless and electrodeposition techniques. We used Ag to provide a thin but electronically conducting layer for Ni electrodeposition, deposited by an electroless process to form Ni/Ag/GDC anodes. This is part of our efforts to fabricate anodes by metallizing, and a continuation from our previous study in this direction [22]. The fabrication of the scaffold provides additional means of microstructural control, since modification of the screen printing ink with pore formers to control porosity is feasible. In this paper, we present a study with a GDC scaffold to fabricate electroless and electrodeposited Ni/Ag/GDC anodes, assessing electrochemical performance using symmetrical cells and a fuel cell.

Experimental

GDC ink and scaffold preparation

The GDC ink was prepared based on formulations developed by Somalu [31] and used in our previous studies [20,32]. $Ce_{0.9}Gd_{0.1}O_{1.95}$ powder (Fuel Cell Materials) and dispersant (Hypermer KD15) were thoroughly mixed with ethanol using ball milling for 24 h. After milling the mixture was dried in an oven at 90 °C for 24 h. Then, terpineol solvent (Sigma Aldrich) and ethylcelulose N7 grade binder (IMCD UK/Hercules) were added into the milled mixture and stirred continuously to form an ink. The ink was homogenized using a triple roll mill (EXAKT, 80E, Germany) for 20 min. The ink preparation is summarized in Fig. 1.

The GDC scaffold was screen printed onto an 8 mol %-yttria-stabilized zirconia disc with thickness of 290 μm (8YSZ, Fuel Cell Materials). The scaffolds were sintered at

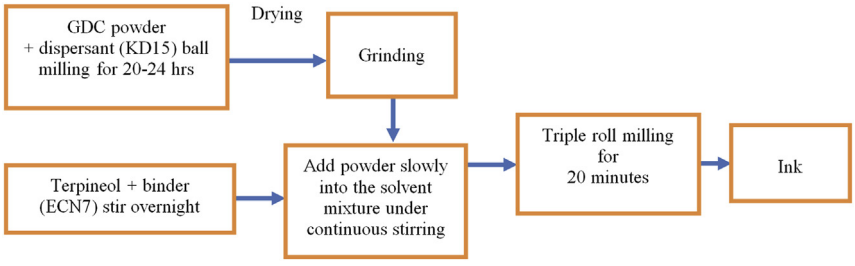

Fig. 1 – Flowchart of GDC ink preparation.

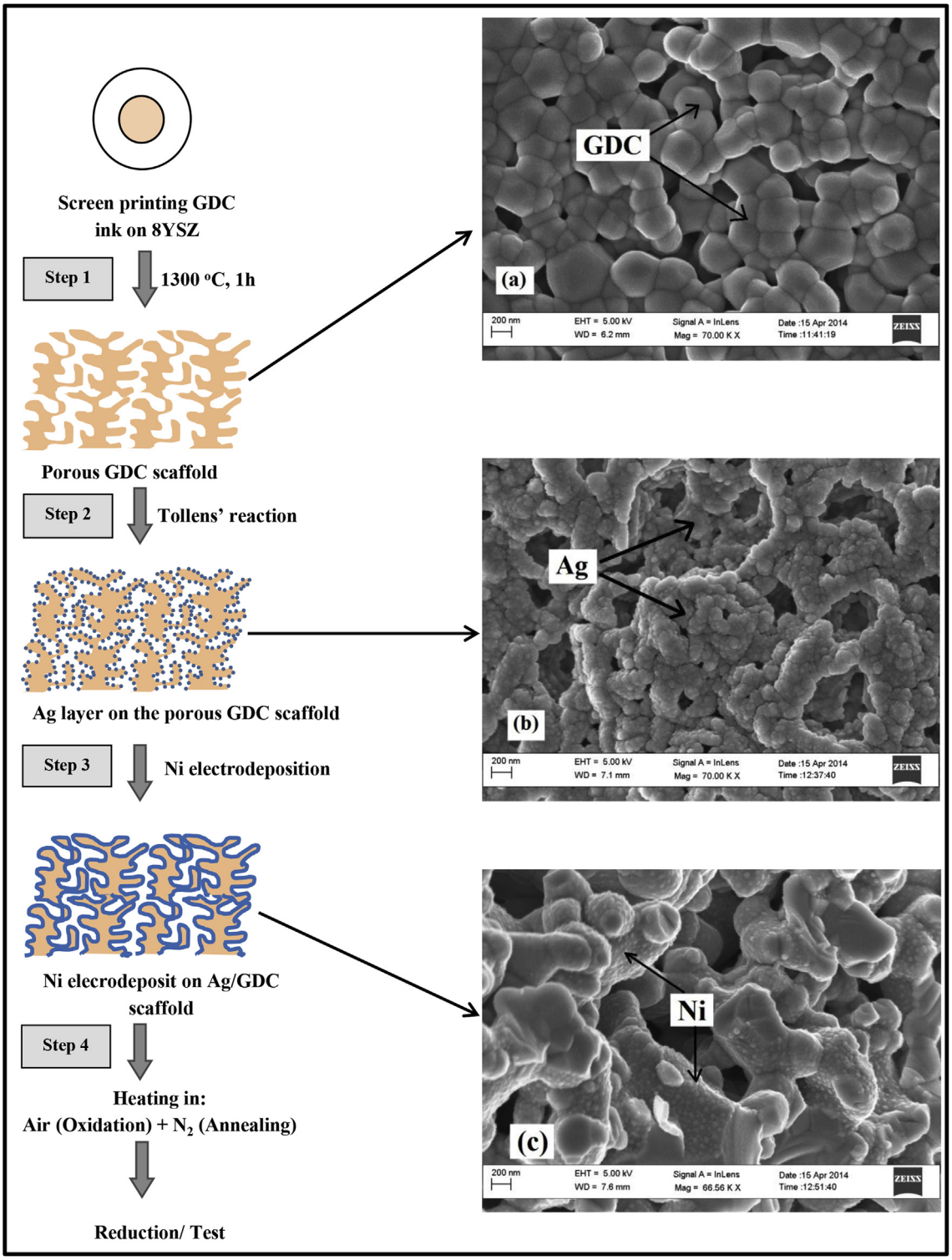

Fig. 2 – Overall processes of electroless and electrolytic deposition of an electrode. The images on the right show the GDC scaffold before and after metallizing process.

1300 °C in air for 1 h. Half cells were fabricated using the same procedures to form nominally identical anodes on both sides of the YSZ disc. To fabricate a full fuel cell, the cathode was screen printed using $(La_{0.6}Sr_{0.4})_{0.95}(Co_{0.2}Fe_{0.8})O_{3-x}$-$Ce_{0.9}Gd_{0.1}O_{1.95}$ (LSCF-GDC, 50:50 wt%) ink (Fuel Cell Materials) and then sintered at 1100 °C for 3 h.

Electroless and electrodeposition

Silver was deposited into the porous GDC scaffold using Tollens' method to provide an electronically conductive layer for electrodeposition. Ni was plated onto the silver layers using an Autolab PGSTAT302N from Ni^{2+} aqueous solution

(Watt's bath) at 70 °C. The full details of the process have been described previously [22]. The overall fabrication method is summarized in Fig. 2.

Fig. 3 shows the symmetrical and fuel cells configurations used in this study. Symmetrical cells of Ag/GDC (S003) and Ni/Ag/GDC (S004) were also prepared to further understand the electrode response and to measure the electrical conductivity of the anode respectively. The metal content was determined by the weight change after metal incorporation. The final compositions of the cells are listed in Table 1. A silver paste and platinum mesh were used as the current collector for the fuel cell and symmetrical cell respectively. Both symmetrical and fuel cells were heated in air to oxidize Ni before they were annealed in N_2 and then reduced in 10 vol% H_2 – 90 vol% N_2 at 600 °C to minimize the microstructural changes in the nickel-metal layer.

DC conductivity

The DC electrical conductivity of an electrodeposited Ni/Ag/GDC (S004) anode was measured under reducing atmospheres of humidified-10 vol% H_2 (balance N_2) at 500–750 °C after pre-oxidation and annealing in N_2 (as described in Section Electroless and Electrodeposition). The conductivity data was collected using the Van der Pauw method by connecting the 4-point probe to an Autolab PGSTAT302N.

Characterization procedure

The electrochemical performance of symmetrical cells with and without Ni-electrodeposit (S001 and S003), including a fuel cell (S002) were measured. In symmetrical cell mode, impedance spectroscopy was used to study anode performance from 600 to 750 °C in humidified-H_2 (10–97 vol% H_2, 3 vol% H_2O). The impedance data were obtained using a potentiostat (Autolab PGSTAT302N), in the frequency range 10^{-1} – 10^5 Hz using an AC signal amplitude of 20 mV and 10 mV for symmetrical and fuel cell modes respectively. Experiments were performed using a two-electrode configuration in the temperature range 550–750 °C in fuel cell mode at various concentrations of humidified H_2 and humidified syngas (15 vol% H_2: 25 vol% CO).

The microstructure of the electrodes was examined using a Scanning Electron Microscopy (LEO Gemini 1525 FEGSEM) and EDX was performed using a JEOL-6400.

Table 1 – Details of YSZ electrolyte-supported electroless and electrodeposited cells prepared in this study.

Code	Cell composites	Cell composition (%vol)
S001	Symmetrical cell: Ni/Ag/GDC	7.5/15.1/77.5
S002	Fuel cell: Anode:Ni/Ag/GDC	3.3/21.1/75.6
	Cathode: LSCF/GDC	50/50[a]
S003	Symmetrical cell: Ag/GDC	18.9/81.1
S004	Symmetrical cell: Ni/Ag/GDC	3.5/24.7/71.8

[a] % wt.

Results and discussion

Fig. 2 depicts the SEM images of the porous GDC scaffold before and after metallizing. The porosity of the GDC originated in part from the combustion of organic compounds in the GDC ink (Fig. 2a). The value of open porosity for the electrodeposited Ni/GDC was about 50–53 vol% with pore diameters around 100–400 nm. The porosity of the scaffold was calculated from its density, obtained from the mass and volume, and then compared to the theoretical GDC density (7.21 g cm^{-3}).

Fig. 2b depicts a uniform coverage of Ag metal onto the GDC scaffold as well as a layer of Ni formed after electrodeposition (Fig. 2c). Around 1 h was required to metallize the GDC scaffold with both Ag and Ni; around 7 times faster than current impregnation methods (5 cycles of 0.5 h of decomposition at 500 °C and ~1 h for heating and cooling) leading to ~7 vol% of Ni incorporation in the scaffold [20]. The metal content of the cells prepared in this study were obtained by weight difference (Table 1) with a measurement uncertainty in the nickel content up to 25% linked to the instrument accuracy of 0.1 mg and the relatively low metal content. The amount of electrodeposited Ni in the porous GDC scaffolds varied from one cell to another, which may reflect variability in the electrodeposition technique and/or error in the measurement. Despite this uncertainty, the electrodes showed an adequate electrical conductivity (see below) with Ni contents lower than those reported in the literature, which are in the

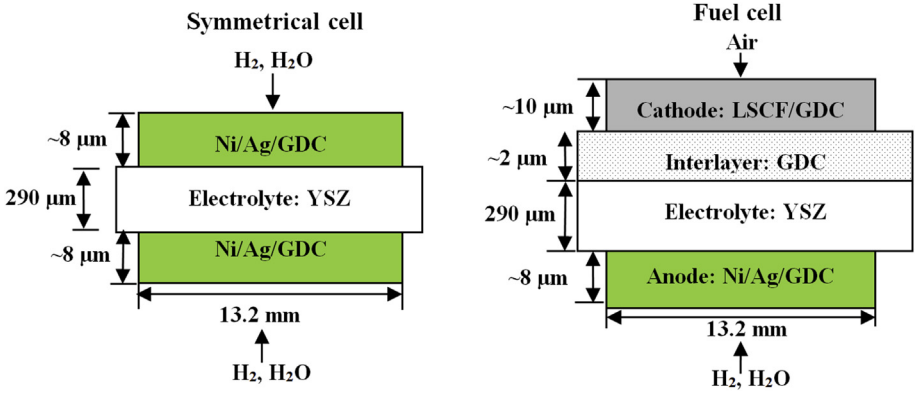

Fig. 3 – Symmetrical and fuel cell configurations used.

range of 20–60 vol% [26,33,34]. The amount of Ni in cell S001 (7.5 vol%) almost reached the same amount of Ni as that obtained using the impregnation method (8.2–13 vol%) [16,35], however with a significantly faster fabrication method and comparable formation of Ni particles (will be shown later in Figs. 10a and 11a).

Conductivity of electrodeposited Ni/Ag/GDC

Fig. 4 presents the conductivity of S004. Also shown in this figure is the electronic conductivity of Ni and Ag metals [36] as well as GDC [37] for reference. The conductivity decreased to 19 S cm^{-1} when the temperature was increased to 750 °C; indicating the metallic nature of the electrode. This value is lower than values reported in the literature (150–620 S cm^{-1}) for electrodes with two to three times higher Ni loading. Although Ni islands in the scaffold limit the electronic conductivity of the electrode, the MIEC properties of GDC in reducing atmospheres could help the conductivity of Ni islands during the measurement [5,38,39]. Furthermore, the contribution of the Ni network on the surface of the electrode (Fig. 10b) to the electronic conductivity needs to be considered in interpreting the Van der Pauw data. Despite the relatively small amounts of metal, the conductivity of the metallized electrode obtained in this study was comparable to the value achieved by combustion synthesized Ni/YSZ (20 S cm^{-1}) with 30 vol% of Ni [40], though not as good as that achieved by Ni/YSZ and Ni/GDC cermets using mechanical mixing (~400 S cm^{-1}, 30–40 vol% Ni) [33,41] and conventional impregnation methods with higher Ni fractions (600–900 S cm^{-1}, 12–16 vol% Ni) [20,42].

Symmetrical cell mode measurements

Two semicircles were observed in the impedance spectra at most temperatures and atmospheres. The values of polarization resistance were estimated by fitting the data to the equivalent electrical circuit shown in Fig. 5. The intercept of the impedance spectra with the real axis at high frequencies corresponds to the ohmic resistance (R_{ohm}). The total area specific resistance (ASR) of the electrode was calculated by the difference of the low frequency intercept of the impedance curve with the real axis and the R_{ohm}. Then the value was extracted from the fitting and normalized by dividing by two and multiplying by the electrode area.

Fig. 6 indicates a relatively constant R_{ohm} at the same temperature with varying atmospheres. As expected, at higher temperatures R_{ohm} decreases from 8.0 to 5.4 Ω (600–750 °C), since the ionic conductivity of the electrolyte is thermally activated. The values of experimental R_{ohm} were higher than the expected values calculated from the YSZ thickness and known conductivities. This difference might be due to contact resistance, and/or an ohmic contribution from the GDC scaffold, and/or a contribution from a reaction layer at the GDC-YSZ interface [43]. This interdiffusion layer (GDC-YSZ) may create lower ion conductivity, almost two orders of magnitude lower than that of YSZ and GDC at 800 °C [44].

The total ASR, which characterizes the electrochemical performance of the electrodes, are tabulated in the inset tables of Fig. 7 and Fig. 8. The low frequency impedance response, R_l was observed to dominate the total ASR at all concentrations of H_2 and at different temperatures. The lowest total ASR reached 1.12 Ω cm^2 at 750 °C in 97 vol% H_2. The total ASR obtained in this study is higher than state of the art conventional and impregnated Ni/GDC and Ni/YSZ cermets in the literature, which are usually in the range of 0.15–0.35 Ω cm^2 [20,34,45–47]. Although a faster metallization

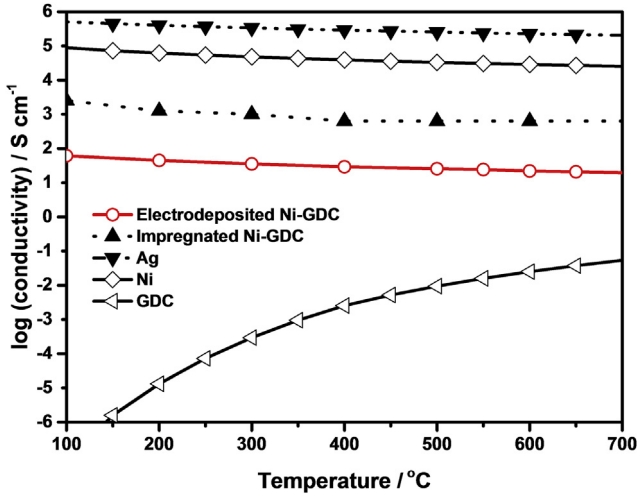

Fig. 4 – Temperature dependence of the conductivity of an electrodeposited electrode (S004) as measured by the Van der Pauw method. The conductivity data was normalized to the thickness of the S004 (7.1 μm). The line obtained in this study was extrapolated at temperatures <500 °C. Also shown in the graph are the conductivity of Ni and Ag metals, and impregnated 12 vol%-Ni/GDC [20].

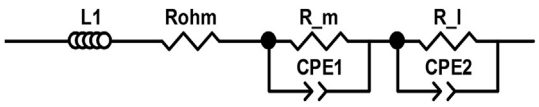

Fig. 5 – The corresponding equivalent circuit used for data fitting in this study.

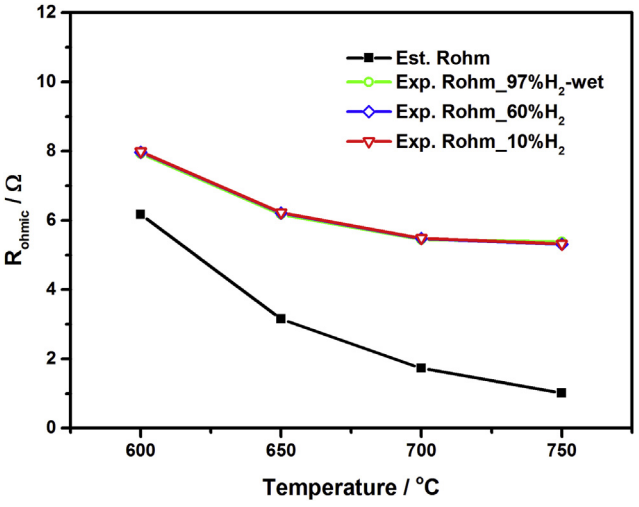

Fig. 6 – Estimated and experimental R_{ohm} of the YSZ electrolyte.

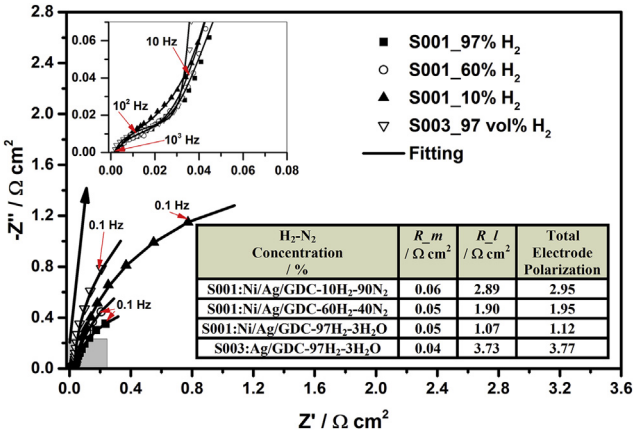

H_2-N_2 Concentration / %	*R_m* / Ω cm²	*R_l* / Ω cm²	Total Electrode Polarization
S001:Ni/Ag/GDC-10H_2-90N_2	0.06	2.89	2.95
S001:Ni/Ag/GDC-60H_2-40N_2	0.05	1.90	1.95
S001:Ni/Ag/GDC-97H_2-3H_2O	0.05	1.07	1.12
S003:Ag/GDC-97H_2-3H_2O	0.04	3.73	3.77

Fig. 7 – Impedance spectra (0.1–10^5 Hz) for the symmetrical cells of S001 (Ni/Ag/GDC) operating at 750 °C in different concentrations of H_2–N_2; and S003 (without Ni) at humidified 97 vol% H_2 (impedance data was normalized to zero). Insets: the graph presents the intermediate frequency behavior of the symmetrical cells, and the table lists the polarization resistance of the electrodes in different atmospheres.

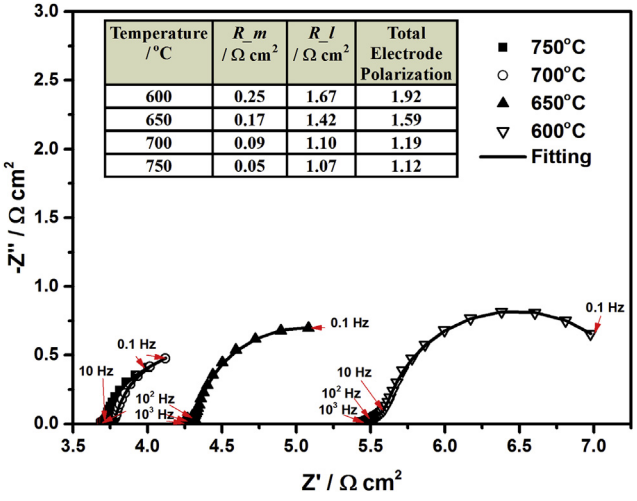

Temperature / °C	*R_m* / Ω cm²	*R_l* / Ω cm²	Total Electrode Polarization
600	0.25	1.67	1.92
650	0.17	1.42	1.59
700	0.09	1.10	1.19
750	0.05	1.07	1.12

Fig. 8 – Impedance spectra (0.1–10^5 Hz) for S001 operating at 97 vol% H_2 under different ranges of temperatures. The inset table shows the total polarization of the electrode at different temperatures.

process of the scaffolds has been demonstrated in this study, it must be noted that the amount and distribution of Ni electrodeposited in the scaffold (7.5 vol%) still requires further optimization before state of the art electrode performance can be achieved. However, this work demonstrates the promise of using electroless and electrodeposition technique for the fabrication of scaffold electrodes.

Fig. 7 displays the effect of H_2 concentration on the complex impedance spectra on S001 and S003 cells (impedance data was normalized to zero) at fixed T = 750 °C. The polarization associated with the intermediate-frequencies arc (10^2–10^3 Hz), *R_m* was observed to be constant at 750 °C in all H_2 concentrations with a value of 0.06 ± 0.01 Ω cm² for S001. A blank symmetrical cell (without Ni, S003), was prepared to measure the electrochemical response of the Ag/GDC scaffold. The *R_m* value of S003 (0.04 Ω cm²) was very close to the values attained in S001, and these values are in accordance to those reported in the literature, typically at <0.1 Ω cm² [48,49]. This is clearly shown by the inset of Fig. 7. In Fig. 8, the *R_m* values significantly decreased from 0.25 to 0.05 Ω cm² when the temperature was increased to 750 °C. These results suggest that the *R_m* was associated with the charge transfer kinetics of hydrogen oxidation at the GDC scaffold.

The low-frequency (<10^2 Hz) arcs were always larger than the intermediate-frequency arcs, and became more significant at low temperatures and low H_2 concentrations as shown in Figs. 7 and 8 respectively. The lowest low-frequency polarization (*R_l*) obtained in this study was 1.07 Ω cm² for 97 vol % H_2 at 750 °C. However, this value is higher than those reported for GDC-impregnated Ni [50], Ni/GDC cermets [34] and Ni-impregnated GDC [20] ranging from 0.1 to 0.4 Ω cm² at temperatures of 690–800 °C. There are several reasons that could explain these observations:

(i) The high *R_l* values could be linked to the limited electronic conductivity of the electrodes, closely related to the amount of metal deposited and the mixed conductivity of GDC. The value of *R_l* for S003 is three times higher than S001 in the same operating conditions, but with no Ni. This indicates that the electronic conductivity of the GDC scaffold contributes to the electrochemical activity.

(ii) The "chemical capacitance" effect that originates from the variation in the oxygen non-stoichiometry (oxygen vacancies) of GDC in reducing atmospheres, complicates the interpretation of the *R_l* data [7,51].

(iii) The contribution of diffusional processes to the *R_l* cannot be ignored as the *R_l* changed with gas composition (Fig. 7). This is probably attributed to: (1) the diffusion of reactant gas to and reaction products from the reaction sites (TPB and 2 PB) in the porous scaffold [52]; (2) Knudsen effects due to the small pore size of the scaffold (~0.25 μm) [49,53]; and/or (3) gas conversion impedance (sensitive to gas composition and temperature) [34,48,54].

Further investigation to resolve these effects is on-going.

The slope of the Arrhenius plots of the electrode polarization resistances (*R_m* and *R_l*) were used to calculate the activation energy for S001 and S003 as depicted in Fig. 9. From the inset table (Fig. 9), the activation energy for *R_m* changed from 1.49 to 0.85 eV (97 vol% – humidified H_2) when small amounts of Ni were added to the GDC scaffold. The activation energy for *R_m* of S001 did not show any significant variation (0.85 ± 0.03 eV) at different concentrations of humidified H_2–N_2 (10–97 vol%). This shows that the kinetics of hydrogen oxidation on the surface of the electrode is improved by adding Ni.

For *R_l*, the activation energies were lower than for *R_m*, and significantly decreased from 0.7 to 0.19 ± 0.04 eV when Ni was added. This may be attributed to the limited electronic conductivity of the GDC scaffold and/or diffusional processes among other effects [55,56]. The small change in the activation energies of *R_l* with temperature (600–750 °C) might be

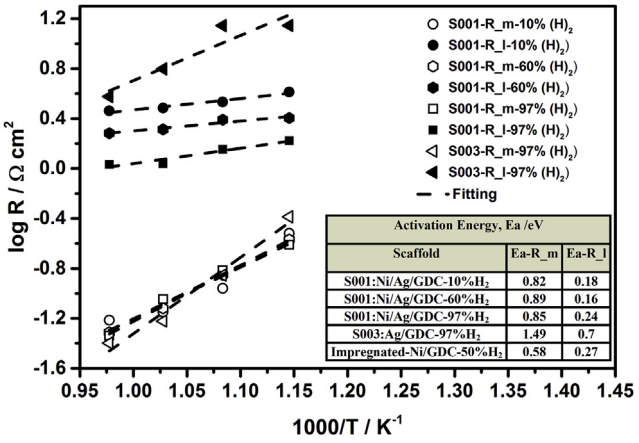

Fig. 9 – Arrhenius plots of the electrode ASR associated with intermediate- (*R_m*) and low-frequency (*R_l*) polarization over the range of temperature and in humidified H_2 (10–97 vol% H_2) for symmetrical cells (S001 and S003).

attributed to surface diffusion and/or adsorption/dissociation of hydrogen species. These are restricted by the conductivity of the GDC scaffold [34,57]. However, further investigation is required to understand this behavior. Overall, the activation energy obtained in this study is comparable to the values reported in the literature with different fabrication methods and anodes (see Table 2).

The microstructure of S001 was examined after electrochemical testing (see Fig. 10). Since there was not enough Ni (7.5 vol%) deposited inside the scaffold to form a continuous film, individual nano-particles of Ni could be observed (Fig. 10a). The Ni distribution and particle sizes (0.05–0.2 μm) are similar to the electrode fabricated by five cycles of the impregnation process (Fig. 11a). Furthermore these particle sizes are considerably smaller than those found in the conventional powder mixing method (1.4–5 μm) [62,63]. This shows that decoupling scaffold fabrication and metal incorporation into the scaffold provides independent control of metal particle size, porosity and TPB density compared to conventional electrodes fabrication (powder mixing). Percolating and homogenous Ni distribution inside the electrodes could be achieved with 50 vol% and 10–20 vol% of Ni by conventional and impregnated electrodes respectively, much higher than the amount of Ni in this study. The challenge to the method proposed here is to increase the amount of Ni added into the GDC pores at lower temperatures (≤70 °C) and with greater speed than the impregnation method. Fig. 10b displays a Ni network on the GDC surface. If this had formed throughout the porous GDC scaffold, it would have provided better electronic pathways from the reaction sites to the current collector. Moreover, the thickness of the scaffold obtained in this study is about 7 μm (Fig. 10c), within the electrochemically active reaction limit (≤10 μm) [64,65]; increasing its thickness may further improve the overall performance.

Under the experimental conditions, silver does not alloy with nickel [66,67] and does not have a high wettability on oxide substrates [68]. Ag films on YSZ become thermally unstable and eventually the film segregates and agglomerates to form isolated islands at high temperatures [69,70]. These islands are clearly shown in Fig. 11b when a Ni/Ag film was heated in air at 800 °C for 1 h. The anode is usually pre-oxidized at high temperature and annealed in nitrogen before its measurement in reducing atmospheres (Step 4 in Fig. 2). The identification of elements in Figs. 10 and 11 was possible in combination with the results from EDX (not shown). In the areas analyzed (Fig. 10), despite the initial presence of silver (15.1 vol%), this metal was not detected (EDX detection limit >0.05 vol%). This suggests that the Ag evaporated during operation at high temperatures, as observed by Wang et al. [68] in air. Evaporation of Ag might be further exacerbated in reducing atmospheres [71].

Table 2 – Comparison of activation energy for different anode materials and fabrication routes.

Anode composition	Fabrication method	Activation energy for *R_m* (eV)	Activation energy for *R_l* (eV)	Reference
Ni/GDC	Impregnation			[16]
(96.5/3.5 vol%)		0.84		
(91.5/8.5 vol%)		0.76		
Ni/YSZ				
(83/17 vol%)		1.03		
(79/21 vol%)		0.82		
Ni/GDC	Sol–gel	1.58–1.93		[34]
Ni/GDC	Spray pyrolysis	1.45		[58]
(49/51 vol%)				
SFMO/LSGM*	Impregnation	0.60	0.77	[59]
(symmetrical cell)				
Ni/GDC	Impregnation	0.65 ± 0.15	0.23–0.34	[20]
(11.6/88.4 vol%)				
Ni/YSZ	Screen printing	0.9–1.1	1.2–1.6	[60]
(40/60 vol%)				
Ni/YSZ	(DK-SOFC project)	1.1	1.6	[61]
Ni/Ag/GDC	Electroless & Electrodeposition	0.85 ± 0.03	0.19 ± 0.03	This study
(7.5/15.1/77.4 vol%)				

SFMO/LSGM = $SrFe_{0.75}Mo_{0.25}O_{3-\delta}/La_{0.9}Sr_{0.1}Ga_{0.8}Mg_{0.2}O_{3-\delta}$.

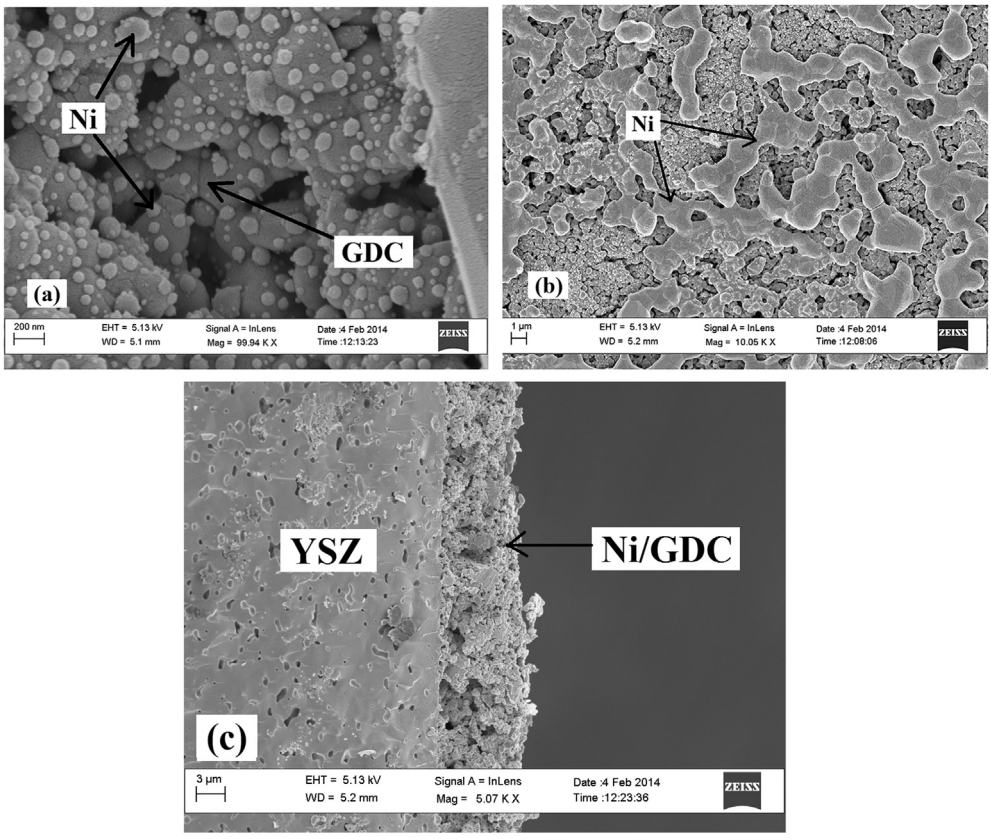

Fig. 10 – After test characterization (S001) at 600–750 °C and different H_2 concentrations: (a) higher magnification view of the Ni/GDC scaffold interior, (b); surface of the Ni/GDC scaffold, and (c) cross section of the electrode.

Fuel cell mode measurements

As a proof of fuel cell concept using electrodeposited Ni/Ag/GDC, S002 was operated under 50 vol% H_2-50 vol% N_2 and syngas at 750 °C. The voltage and power densities as a function of current density are shown in Fig. 12a. Most losses were ohmic in nature, dominated by the thick YSZ electrolyte (290 µm). Reflecting this, the maximum power densities were modest and reached about 56 mW cm^{-2} at ~0.7 V under 50 vol% H_2-50 vol% N_2 with an ASR including electrolyte and electrodes of 4.79 Ω cm^2. This value is consistent with the total cell polarization obtained from the total impedance in Fig. 12b of 4.81 Ω cm^2. The maximum power density achieved by S002 operating under syngas was 33 mW cm^{-2} at ~0.5 V. Future work will focus on depositing these electrodes onto much thinner electrolytes.

Conclusions

The successful deposition of silver and nickel by electroless and electrolytic methods into porous GDC scaffold was achieved. This technique is much faster than conventional impregnation methods, however the amount and

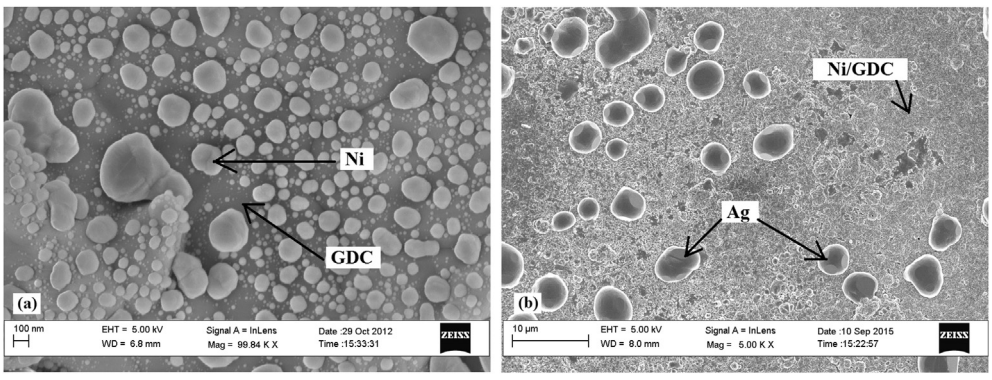

Fig. 11 – (a) Image of 5-cycles impregnation Ni/GDC from our own work [20]; (b) segregation and agglomeration of Ag at the surface of the electrodeposited Ni/GDC scaffold after heating at 800 °C in air.

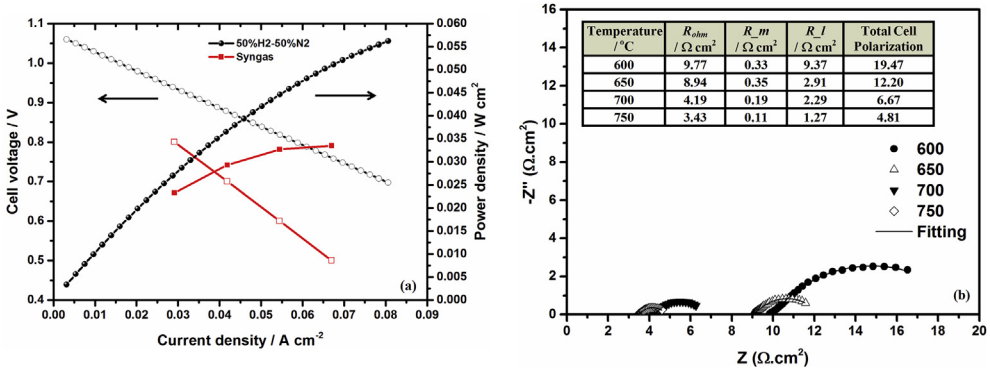

Fig. 12 – Fuel cell (S002) operation (a) voltage and power density curves vs. current density operating in 50 vol% H_2 – 50 vol% N_2 and syngas at 750 °C; (b) impedance spectra (0.1–10^5 Hz) operating at 50 vol% H_2 – 50 vol% N_2 at different temperatures. The inset table shows the polarization resistance of the cell at different temperatures.

distribution of Ni deposited in the scaffold needs to be further optimized to achieve state of the art electrode performance. Metallizing the scaffold took place at temperatures lower than 100 °C, well below the temperatures used to process impregnated anodes. After operation at higher temperatures (600–750 °C), there is evidence for the formation of islands of nickel inside the scaffold that increase the TPB of the electrode, when used on a mixed conducting GDC scaffold. On the electrode surface, the nickel forms an interconnected network that can be used as a current collector. The main role of Ag is to provide a conductive surface for Ni electrodeposition. Its contribution to the electronic conductivity of the scaffold and electrochemical reactions might be minimal. In regions analyzed by EDX, silver was not detected, probably indicating agglomeration in other regions, migration to the current collector or evaporation due to high temperature and reducing environments.

In the impedance measurements, there were two types of electrode response. The first appeared at intermediate frequencies (100–1000 Hz), and the second at low frequencies (<100 Hz), showing a polarization resistance of 0.05 Ω cm^2 and 1.07 Ω cm^2 respectively, with a total ASR of 1.12 Ω cm^2 at 750 °C (symmetrical cell mode, S001). The activation energy of the electrode at *R_m* is always higher than at *R_l*, being 0.85 ± 0.03 eV and 0.19 ± 0.03 eV respectively. The cells are able to be operated under both H_2 and syngas (fuel cell mode). Whilst the distribution and amount of Ni needs to be further improved, this fabrication technique offers an alternative for processing SOFC anodes, especially for large scale production.

Acknowledgment

The authors would like to acknowledge UiTM Slab, Ministry of Education Malaysia Scholarship and EPSRC through project "Advancing Biogas Utilization through Fuel Flexible SOFC" (EP/I037016/1) for funding this work.

REFERENCES

[1] Zhu WZ, Deevi SC. A review on the status of anode materials for solid oxide fuel cells. Mater Sci Eng A 2003;362:228–39. http://dx.doi.org/10.1016/S0921-5093(03)00620-8.

[2] Novosel B, Marinšek M, Maček J. Deactivation of Ni-YSZ material in dry methane and oxidation of various forms of deposited carbon. J Fuel Cell Sci Technol 2012;9. http://dx.doi.org/10.1115/1.4007272. 061003-1–061003-7.

[3] Alzate-Restrepo V, Hill JM. Carbon deposition on Ni/YSZ anodes exposed to CO/H2 feeds. J Power Sources 2010;195:1344–51. http://dx.doi.org/10.1016/j.jpowsour.2009.09.014.

[4] Atkinson A, Barnett S, Gorte RJ, Irvine JTS, McEvoy AJ, Mogensen M, et al. Advanced anodes for high-temperature fuel cells. Nat Mater 2004;3:17–27. http://dx.doi.org/10.1038/nmat1040.

[5] Chueh WC, Hao Y, Jung W, Haile SM. High electrochemical activity of the oxide phase in model ceria-Pt and ceria-Ni composite anodes. Nat Mater 2012;11:155–61. http://dx.doi.org/10.1038/nmat3184.

[6] Jiang SP, Chan SH. A review of anode materials development in solid oxide fuel cells. J Mater Sci 2004;39:4405–39. http://dx.doi.org/10.1023/B:JMSC.0000034135.52164.6b.

[7] Chueh WC, Lai W, Haile SM. Electrochemical behavior of ceria with selected metal electrodes. Solid State Ion 2008;179:1036–41. http://dx.doi.org/10.1016/j.ssi.2007.12.087.

[8] Babaei A, Zhang L, Liu E, Jiang SP. Performance and carbon deposition over Pd nanoparticle catalyst promoted Ni/GDC anode of SOFCs in methane, methanol and ethanol fuels. Int J Hydrogen Energy 2012;37:15301–10. http://dx.doi.org/10.1016/j.ijhydene.2012.07.089.

[9] Zupan K, Marinsek M. Microstructure development of the Ni-GDC anode material for IT-SOFC. Mater Technol 2012;46:445–51. doi:UDK 546:66.017:669.018.95.

[10] Sun C, Stimming U. Recent anode advances in solid oxide fuel cells. J Power Sources 2007;171:247–60. http://dx.doi.org/10.1016/j.jpowsour.2007.06.086.

[11] Marina OA, Mogensen M. High-temperature conversion of methane on a composite gadolinia-doped ceria–gold electrode. Appl Catal A Gen 1999;189:117–26. http://dx.doi.org/10.1016/S0926-860X(99)00259-8.

[12] Zhang L, Jiang SP, He HQ, Chen X, Ma J, Song XC. A comparative study of H2S poisoning on electrode behavior of Ni/YSZ and Ni/GDC anodes of solid oxide fuel cells. Int J

Hydrogen Energy 2010;35:12359–68. http://dx.doi.org/10.1016/j.ijhydene.2010.08.067.
[13] Papadam T, Goula G, Yentekakis IV. Long-term operation stability tests of intermediate and high temperature Ni-based anodes' SOFCs directly fueled with simulated biogas mixtures. Int J Hydrogen Energy 2012;37:16680–5. http://dx.doi.org/10.1016/j.ijhydene.2012.02.147.
[14] Rosch B, Tu H, Stormer AO, Muller AC, Stimming U. Electrochemical characterization of Ni-Ce(0.9)Gd(0.1)O(2-δ) for SOFC anodes. Solid State Ion 2004;175:113–7. http://dx.doi.org/10.1016/j.ssi.2004.09.022.
[15] Zheng LL, Wang X, Zhang L, Wang J-Y, Jiang SP. Effect of Pd-impregnation on performance, sulfur poisoning and tolerance of Ni/GDC anode of solid oxide fuel cells. Int J Hydrogen Energy 2012;37:10299–310. http://dx.doi.org/10.1016/j.ijhydene.2012.03.105.
[16] Jiang SP, Zhang S, Zhen YD, Koh AP. Performance of GDC-impregnated Ni anodes of SOFCs. Electrochem Solid-State Lett 2004;7:A282–5. http://dx.doi.org/10.1149/1.1783112.
[17] Jiang SP, Zhang S, Zhen YD, Wang W. Fabrication and performance of impregnated Ni anodes of solid oxide fuel cells. J Am Ceram Soc 2005;88:1779–85. http://dx.doi.org/10.1111/j.1551-2916.2005.00362.x.
[18] Ruiz-Trejo E, Irvine JTS. Electrolysis of CO2 in a proton conducting membrane. Solid State Ion 2013;252:157–64. http://dx.doi.org/10.1016/j.ssi.2013.05.021.
[19] Lee S-I, Vohs JM, Gorte RJ. A study of SOFC anodes based on Cu–Ni and Cu–Co bimetallics in CeO(2)-YSZ. J Electrochem Soc 2004;151. http://dx.doi.org/10.1149/1.1774184. A1319–23.
[20] Lomberg M, Ruiz-Trejo E, Offer G, Brandon NP. Characterization of Ni-infiltrated GDC electrodes for solid oxide cell applications. J Electrochem Soc 2014;161:F899–905. http://dx.doi.org/10.1149/2.0501409jes.
[21] Jung S, Lu C, He H, Ahn K, Gorte RJ, Vohs JM. Influence of composition and Cu impregnation method on the performance of Cu/CeO(2)/YSZ SOFC anodes. J Power Sources 2006;154:42–50. http://dx.doi.org/10.1016/j.jpowsour.2005.04.018.
[22] Ruiz-Trejo E, Atkinson A, Brandon NP. Metallizing porous scaffolds as an alternative fabrication method for solid oxide fuel cell anodes. J Power Sources 2015;280:81–9. http://dx.doi.org/10.1016/j.jpowsour.2015.01.091.
[23] Ruiz-Trejo E, Azad AK, Irvine JTS. A 60-second microwave-assisted synthesis of nickel foam and its application to the impregnation of porous scaffolds. J Electrochem Soc 2014;162. http://dx.doi.org/10.1149/2.0531503jes. F273–9.
[24] Chitvoranund N, Jiemsirilers S, Kashima DP. Effects of surface treatments on adhesion of silver film on glass substrate fabricated by electroless plating. J Aust Ceram Soc 2013;49:62–9. doi:10.4028, www.scientific.net/AMR.664.566.
[25] Rao C, Trivedi D. Chemical and electrochemical depositions of platinum group metals and their applications. Coord Chem Rev 2005;249:613–31. http://dx.doi.org/10.1016/j.ccr.2004.08.015.
[26] Pratihar SK, Dassharma A, Maiti HS. Properties of Ni/YSZ porous cermets prepared by electroless coating technique for SOFC anode application. J Mater Sci 2007;42:7220–6. http://dx.doi.org/10.1007/s10853-007-1497-x.
[27] Nwosu NO, Davidson AM, Hindle CS. Effect of sodium dodecyl sulphate on the composition of electroless nickel – yttria stabilized zirconia coatings. Adv Chem Eng Sci 2011;01:118–24. http://dx.doi.org/10.4236/aces.2011.13018.
[28] Baba NB, Davidson A. Investigation of Ni-YSZ SOFC anode fabricated via electroless nickel co-deposition. Procedia Eng 2011;23:474–8. http://dx.doi.org/10.1016/j.proeng.2011.11.2533.
[29] Jung S, Gross MD, Gorte RJ, Vohs JM. Electrodeposition of Cu into a highly porous Ni/YSZ cermet. J Electrochem Soc 2006;153:A1539–43. http://dx.doi.org/10.1149/1.2208908.
[30] Jung S-W, Vohs JM, Gorte RJ. Preparation of SOFC anodes by electrodeposition. J Electrochem Soc 2007;154:B1270–5. http://dx.doi.org/10.1149/1.2790280.
[31] Somalu MR, Yufit V, Brandon NP. The effect of solids loading on the screen-printing and properties of nickel/scandia-stabilized-zirconia anodes for solid oxide fuel cells. Int J Hydrogen Energy 2013;38:9500–10. http://dx.doi.org/10.1016/j.ijhydene.2012.06.061.
[32] Boldrin P, Ruiz-Trejo E, Yu J, Gruar RI, Tighe CJ, Chang K-C, et al. Nanoparticle scaffolds for syngas-fed solid oxide fuel cells. J Mater Chem A 2014;3:3011–8. http://dx.doi.org/10.1039/C4TA06029F.
[33] Muecke UP, Graf S, Rhyner U, Gauckler LJ. Microstructure and electrical conductivity of nanocrystalline nickel- and nickel oxide/gadolinia-doped ceria thin films. Acta Mater 2008;56:677–87. http://dx.doi.org/10.1016/j.actamat.2007.09.023.
[34] Macedo DA, Figueiredo FML, Paskocimas CA, Martinelli AE, Nascimento RM, Marques FMB. Ni–CGO cermet anodes from nanocomposite powders: microstructural and electrochemical assessment. Ceram Int 2014;40:13105–13. http://dx.doi.org/10.1016/j.ceramint.2014.05.010.
[35] Gore CM, Lee KT, Yoon HS, Wachsman ED. Porous GDC scaffold anodes for lower temperature, hydrocarbon-fueled solid oxide fuel cells. ECS Trans 2013;50:53–62. http://dx.doi.org/10.1149/05027.0053ecst.
[36] Van Sciver SW. Low-temperature materials properties. Helium Cryog. Internatio, New York. New York: Springer; 2012. p. 17–58. http://dx.doi.org/10.1007/978-1-4419-9979-5.
[37] Steele B. Appraisal of Ce(1–y)Gd(y)O(2–y/2) electrolytes for IT-SOFC operation at 500 °C. Solid State Ionics 2000;129:95–110. http://dx.doi.org/10.1016/S0167-2738(99)00319-7.
[38] Ruiz-Trejo E, Maier J. Electronic transport in single crystals of Gd-Doped Ceria. J Electrochem Soc 2007;154:B583. http://dx.doi.org/10.1149/1.2722530.
[39] Zhang C, Grass ME, McDaniel AH, DeCaluwe SC, Gabaly El F, Liu Z, et al. Measuring fundamental properties in operating solid oxide electrochemical cells by using in situ X-ray photoelectron spectroscopy. Nat Mater 2010;9:944–9. http://dx.doi.org/10.1038/nmat2851.
[40] Anselmi-Tamburini U, Chiodelli G, Arimondi M, Maglia F, Spinolo G, Munir ZA. Electrical properties of Ni/YSZ cermets obtained through combustion synthesis. Solid State Ionics 1998;110:35–43. http://dx.doi.org/10.1016/S0167-2738(98)00115-5.
[41] Li Y, Xie Y, Gong J, Chen Y, Zhang Z. Preparation of Ni/YSZ materials for SOFC anodes by buffer-solution method. Mater Sci Eng B Solid-State Mater Adv Technol 2001;86:119–22. http://dx.doi.org/10.1016/S0921-5107(01)00683-3.
[42] Tiwari P, Basu S. Ni infiltrated YSZ anode stabilization by inducing strong metal support interaction between nickel and titania in solid oxide fuel cell under accelerated testing. Int J Hydrogen Energy 2013;38:9494–9. http://dx.doi.org/10.1016/j.ijhydene.2012.09.094.
[43] Tsoga A, Gupta A, Stoever D. Performance characteristics of composite film electrolytes for intermediate-temperature solid oxide fuel cells. Ionics (Kiel) 1999;5:175–82. http://dx.doi.org/10.1007/bf02375837.
[44] Tsoga A. Total electrical conductivity and defect structure of ZrO2–CeO2–Y2O3–Gd2O3 solid solutions. Solid State Ion 2000;135:403–9. http://dx.doi.org/10.1016/S0167-2738(00)00477-X.
[45] Lee KT, Vito NJ, Yoon HS, Wachsman ED. Effect of Ni-Gd(0.1)Ce(0.9)O(1.95) anode functional layer composition on

performance of lower temperature SOFCs. J Electrochem Soc 2012;159:F187–93. http://dx.doi.org/10.1149/2.009207jes.
[46] Primdahl S, Mogensen M. Oxidation of hydrogen on Ni/Yttria-stabilized zirconia cermet anodes. J Electrochem Soc 1997;144:3409–19.
[47] Koide H. Properties of Ni/YSZ cermet as anode for SOFC. Solid State Ion 2000;132:253–60. http://dx.doi.org/10.1016/S0167-2738(00)00652-4.
[48] Blennow P, Hjelm J, Klemensø T, Persson ÅH, Ramousse S, Mogensen M. Planar metal-supported SOFC with novel cermet anode. Fuel Cells 2011;11:661–8. http://dx.doi.org/10.1002/fuce.201100029.
[49] Primdahl S, Mogensen M. Gas diffusion impedance in characterization of solid oxide fuel cell anodes. J Electrochem Soc 1999;146:2827. http://dx.doi.org/10.1149/1.1392015.
[50] Wang W, Jiang SP, Tok AIY, Luo L. GDC-impregnated Ni anodes for direct utilization of methane in solid oxide fuel cells. J Power Sources 2006;159:68–72. http://dx.doi.org/10.1016/j.jpowsour.2006.04.051.
[51] Atkinson A, Baron SA, Brandon NP. AC impedance spectra arising from mixed ionic electronic solid electrolytes. J Electrochem Soc 2004;151:E186. http://dx.doi.org/10.1149/1.1690291.
[52] Yeqing F, Jiang Y, Poizeau S, Dutta A, Mohanram A, Pietras JD, et al. Multicomponent gas diffusion in porous electrodes. J Electrochem Soc 2015;162:F613–21. http://dx.doi.org/10.1149/2.0911506jes.
[53] Kishimoto M, Iwai H, Saito M, Yoshida H. Quantitative evaluation of transport properties of SOFC porous anode by random walk process. In: Proc. 14th Int. Heat Transf. Conf. IHTC14; 2010. http://dx.doi.org/10.1149/1.3205731. IHTC14–22495.
[54] Nielsen J, Klemensø T, Blennow P. Detailed impedance characterization of a well performing and durable Ni:CGO infiltrated cermet anode for metal-supported solid oxide fuel cells. J Power Sources 2012;219:305–16. http://dx.doi.org/10.1016/j.jpowsour.2012.07.031.
[55] Tuller H. Semiconduction and mixed ionic-electronic conduction in nonstoichiometric oxides: impact and control. Solid State Ion 1997;94:63–74. http://dx.doi.org/10.1016/S0167-2738(96)00585-1.
[56] Lai W, Haile SM. Impedance spectroscopy as a tool for chemical and electrochemical analysis of mixed conductors: a case study of ceria. J Am Ceram Soc 2005;88:2979–97. http://dx.doi.org/10.1111/j.1551-2916.2005.00740.x.
[57] Primdahl S, Mogensen M. Mixed conductor anodes: Ni as electrocatalyst for hydrogen conversion. Solid State Ion 2002;152–153:597–608. http://dx.doi.org/10.1016/S0167-2738(02)00393-4.
[58] Muecke U, Akiba K, Infortuna A, Salkus T, Stus N, Gauckler L. Electrochemical performance of nanocrystalline nickel/gadolinia-doped ceria thin film anodes for solid oxide fuel cells. Solid State Ion 2008;178:1762–8. http://dx.doi.org/10.1016/j.ssi.2007.10.002.
[59] Meng X, Liu X, Han D, Wu H, Li J, Zhan Z. Symmetrical solid oxide fuel cells with impregnated SrFe(0.75)Mo(0.25)O(3−δ) electrodes. J Power Sources 2014;252:58–63. http://dx.doi.org/10.1016/j.jpowsour.2013.11.049.
[60] Brown M, Primdahl S, Mogensen M. Structure/Performance relations for Ni/Yttria-stabilized zirconia anodes for solid oxide fuel cells. J Electrochem Soc 2000;147:475–85. http://dx.doi.org/10.1149/1.1393220.
[61] Barfod R, Hagen A, Ramousse S, Hendriksen PV, Mogensen M. Break down of losses in thin electrolyte SOFCs. Fuel Cells 2006;6:141–5. http://dx.doi.org/10.1002/fuce.200500113.
[62] Kishimoto M, Lomberg M, Ruiz-Trejo E, Brandon NP. Enhanced triple-phase boundary density in infiltrated electrodes for solid oxide fuel cells demonstrated by high-resolution tomography. J Power Sources 2014;266:291–5. http://dx.doi.org/10.1016/j.jpowsour.2014.05.038.
[63] Lee J-H, Moon H, Lee H-W, Kim J-D, Kim J-D, Yoon K-H. Quantitative analysis of microstructure and its related electrical property of SOFC anode, Ni–YSZ cermet. Solid State Ion 2002;148:15–26. http://dx.doi.org/10.1016/S0167-2738(02)00050-4.
[64] Gorte RJ, Vohs JM. Novel SOFC anodes for the direct electrochemical oxidation of hydrocarbons. J Catal 2003;216:477–86. http://dx.doi.org/10.1016/S0021-9517(02)00121-5.
[65] Fleig J. Solid oxide fuel cell cathodes: polarization mechanisms and modeling of the electrochemical performance. Annu Rev Mater Res 2003;33:361–82. http://dx.doi.org/10.1146/annurev.matsci.33.022802.093258.
[66] Singleton M, Nash P. The Ag–Ni (Silver–Nickel) system. J Phase Equilib 1987;8:119–21. http://dx.doi.org/10.1007/BF02873194.
[67] Liu XJ, Gao F, Wang CP, Ishida K. Thermodynamic assessments of the Ag–Ni binary and Ag–Cu–Ni ternary systems. J Electron Mater 2008;37:210–7. http://dx.doi.org/10.1007/s11664-007-0315-1.
[68] Wang LS, Thiele ES, Barnett SA. Sputter deposition of yttria-stabilized zirconia and silver cermet electrodes for SOFC applications. Solid State Ion 1992;52:261–7. http://dx.doi.org/10.1016/0167-2738(92)90114-5.
[69] Simrick NJ, Kilner JA, Atkinson A. Thermal stability of silver thin films on zirconia substrates. Thin Solid Films 2012;520:2855–67. http://dx.doi.org/10.1016/j.tsf.2011.11.048.
[70] Sharma SK, Spitz J. Hillock formation, hole growth and agglomeration in thin silver films. Thin Solid Films 1980;65:339–50. http://dx.doi.org/10.1016/0040-6090(80)90244-8.
[71] Gavrielatos, Montinaro, Orfanidi, Neophytides. Thermogravimetric and electrocatalytic study of carbon deposition of Ag-doped Ni/YSZ electrodes under internal CH4 Steam reforming conditions. Fuel Cells 2009;9:883–90. http://dx.doi.org/10.1002/fuce.200800181.